Finite temperature vortices in a rotating Fermi gas

S. N. Klimin,* J. Tempere,† and N. Verhelst

TQC, Universiteit Antwerpen, Universiteitsplein 1, B-2610 Antwerpen, Belgium

M. V. Milošević

Departement Fysica, Universiteit Antwerpen,

Groenenborgerlaan 171, B-2020 Antwerpen, Belgium

(Dated: December 2, 2015)

Abstract

Vortices and vortex arrays have been used as a hallmark of superfluidity in rotated, ultracold Fermi gases. These superfluids can be described in terms of an effective field theory for a macroscopic wave function representing the field of condensed pairs, analogous to the Ginzburg-Landau theory for superconductors. Here, we have established how rotation modifies this effective field theory, by rederiving it starting from the action of Fermi gas in the rotating frame of reference. In particular, we show that the moment of inertia that can be attributed to the pairs deviates from the naive expectation that it is twice the moment of inertia of the constituent fermions, which is only realized in the deep BEC regime. Then, we use our macroscopic wave function description to study vortices and the critical rotation frequencies to form them. Phase diagrams for vortex states are derived, and they are in good agreement with available results of the Bogoliubov – De Gennes theory and with experimental data.

*Department of Theoretical Physics, State University of Moldova

†Lyman Laboratory of Physics, Harvard University

I. INTRODUCTION

Vortices and vortex matter in superconductors and superfluid atomic gases are subjects of a great interest since a long time [1]. Stable vortices in superconductors appear under the presence of an external magnetic field. In superfluid atomic Bose and Fermi gases, vortices are stabilized when a trapped gas rotates, because the superfluid cannot support rigid-body rotation [2, 3]. Stable vortices and vortex arrays were successfully generated experimentally in condensates of bosonic [4–7] and fermionic cold atoms [8].

The experimental progress stimulated theoretical efforts to describe physics of vortex formation in rotating trapped quantum gases. Different theoretical methods were applied to describe the physics of the vortex matter in these systems: the Gross-Pitaevskii (GP) equation for Bose gases [9, 10], the Ginzburg - Landau (GL) formalism [11], the Bogoliubov - De Gennes (BdG) theory [12–15] and the superfluid density functional theory [16] for Fermi gases. The first calculation of the critical rotational velocity for a trapped Fermi gas has been performed in Ref. [11] using a thermodynamic calculation of the energy of a vortex state. A similar calculation for the Bose gases was performed earlier in Ref. [17]. The rotating Fermi condensates were investigated using macroscopic hydrodynamic equations in Refs. [18, 19]. In Refs. [20–22], the vortex formation in a rotating trapped Fermi gas is studied using the Bogoliubov - De Gennes (BdG) equations. In Ref. [23], vortex arrays in rotating Fermi condensates are analyzed using the coarse graining method for the BdG equations developed in Ref. [24], and referred to as a local phase density approximation (LPDA) to the BdG equations.

The BdG theory is a powerful tool for a theoretical analysis of superfluid Fermi gases in the BCS-BEC crossover. However, from the computational point of view, solution of the BdG equations for the fermionic wave functions is greatly more involved than the solution of, e. g., the Gross-Pitaevskii equation or any other effective field approach describing the superfluid through a macroscopic wave function. As a result, the application of the BdG formalism is mostly limited to the zero-temperature properties of single-vortex states [12–14], and to circumvent this limitation there has been great interest in the development of effective field theories [24, 27, 29–31] that can describe non-uniform excitations (e. g., vortices, solitons) in finite-temperature Fermi gases in the BCS-BEC crossover. A notable example is the coarse-grained approximation to the static BdG formalism of Ref. [24], which

allowed to extend the analysis to the whole temperature range below T_c. Here we will focus on the finite temperature development of the effective field theory (EFT) developed recently in Refs. [25, 26], based on a gradient expansion of the pairing order parameter at finite temperatures. This development of the EFT is dynamic, accounting for both first-order and second-order time derivatives of the pair field, that allows to treat both equilibrium and time-dependent phenomena in condensed Fermi gases. In particular, the method described in Refs. [25, 26] was applied to solitons in a fermionic superfluid [27], where its advantage becomes clear: an analytic solution to the field equation is available. This approach will be referred to as KTD, and shown to compare successfully to the BdG formalism in the appropriate limit. Comparing this result to the numerical BdG simulations has shown that the effective field theory of [25, 26] is applicable throughout the BCS-BEC crossover except for the combination of the BCS regime and temperatures far below T_c [28].

The goal of the current paper is to incorporate rotation into the KTD effective field theory. This is done (in Sec. II) by including the rotating potential at the level of the fermionic degrees of freedom, and deriving the modified EFT for the macroscopic wave function. As we will show, away from the BEC limit, the rotational moment of inertia of the fermionic pairs, is not merely twice that of the individual atoms. In Sec. III, we show the vortex phase diagrams and determine the critical rotation frequencies as a function of temperature and interaction strength, compare the results with those of Refs. [20, 21, 23] and analyze their connection with the experimental data [8]. Our results are summarized in Sec. IV.

II. EFFECTIVE FIELD ACTION

The KTD approach described in Refs. [25, 26] is based on the path-integral description of the interacting Fermi gas. The Hubbard-Stratonovich transformation is used to introduce the bosonic pair field Ψ, and the action functional for these fields is obtained by integrating out the fermionic degrees of freedom. In the resulting action, a gradient expansion is performed, not around $\Psi = 0$ as in the Ginzburg - Landau approach, but around the coordinate-dependent saddle-point value to be determined self consistently. The bosonic pair field is then interpreted as a macroscopic wave function for the superfluid pair condensate. This approach is valid when Ψ is slowly varying in space and in time, and for Fermi gases with a sufficiently large number of particles or sufficiently strong coupling in order to

ensure $R \gg \xi$, where $R = \left(\hbar/\left(m\omega_0\right)\right)^{1/2}$ is the characteristic scale for the trap potential, and ξ is the characteristic scale of non-uniform excitations, e. g., vortices or solitons. The regimes of validity have been studied in more detail in Ref. [28].

In order to incorporate rotation into this description, we first consider the single-particle Hamiltonian for a fermionic atom with mass m confined to an anisotropic parabolic trap in the rotating frame of reference. The rotation leads to the appearance of the term $\left(-\omega\hat{L}_z\right)$ where ω is the rotation frequency and $\hat{L}_z$ is the z component of the orbital angular momentum of the particle. Therefore the single-particle Hamiltonian in the rotating frame of reference is [32, 33]:

$$H = -\frac{\left(\nabla - i\mathbf{A}\left(\mathbf{r}\right)\right)^2}{2m} + \frac{m\left(\omega_\perp^2 - \omega^2\right)}{2}\left(x^2 + y^2\right) + \frac{m\omega_z^2}{2}z^2, \tag{1}$$

with the "rotational" vector potential

$$\mathbf{A}\left(\mathbf{r}\right) = m\left[\boldsymbol{\omega} \times \mathbf{r}\right], \tag{2}$$

and the rotation vector

$$\boldsymbol{\omega} \equiv \omega\mathbf{e}_z. \tag{3}$$

The effect of rotation results in the appearance of the vector potential (2), for which $\nabla_{\mathbf{r}} \cdot \mathbf{A} = 0$, and also in the softening of the confinement potential through $\omega_\perp^2 \to \omega_\perp^2 - \omega^2$. The trapped atomic configuration can be stable when $\omega_\perp^2 - \omega^2 > 0$. In the context of our earlier assumption of a slowly varying field ($R \gg \xi$), the local density approximation is suitable to take into account the confinement through a coordinate dependent chemical potential:

$$\mu\left(\mathbf{r}\right) = \mu_0 - \frac{m\omega_\perp^2}{2}\left(x^2 + y^2\right) - \frac{m\omega_z^2}{2}z^2. \tag{4}$$

This chemical potential enters the coordinate-dependent fermion density, which is determined from the local number equation. Correspondingly, the confinement potential for a rotating Fermi gas, as follows from (1), will be renormalized as:

$$\mu_\omega\left(\mathbf{r}\right) = \mu_0 - \frac{m\left(\omega_\perp^2 - \omega^2\right)}{2}\left(x^2 + y^2\right) - \frac{m\omega_z^2}{2}z^2. \tag{5}$$

An *ad hoc* method to incorporate the rotational vector potential into the effective field theory of KTD, would be to replace the gradients $\nabla_{\mathbf{r}}$ by the covariant derivatives $\nabla_{\mathbf{r}} - 2iA$. This is similar to the incorporation of the vector potential for a magnetic field in the Ginzburg

- Landau theory for superconductors [34], where the factor 2 in front of A comes from the fact that the Cooper-pair charge is twice the electron charge. This assumption is then based on a formal analogy between the rotation and the external magnetic field. Here, the rotational moment of inertia of the pair plays the role of the charge, which naively may be considered twice that of a single atom since the mass of the pair is twice as large. The aforesaid *ad hoc* method is frequently used, see. e. g., Refs. [23, 32]. However, as we will show, for the rotational case, this is *not substantiated* by the microscopic derivation (as distinct from the magnetic case), except in the BEC limit.

The partition function of a fermionic system with two spin states ($\sigma =\uparrow,\downarrow$) is determined by the path integral over the fermionic fields ,

$$\mathcal{Z} \propto \int \mathcal{D}\left[\bar{\psi},\psi\right] e^{-S}. \tag{6}$$

where the action functional S is given by:

$$S=\int_0^\beta d\tau \int d\mathbf{r}\left[\sum_{\sigma=\uparrow,\downarrow}\bar{\psi}_\sigma\left(\frac{\partial}{\partial\tau}+H-\mu_\sigma\left(\mathbf{r}\right)\right)\psi_\sigma+g\bar{\psi}_\uparrow\bar{\psi}_\downarrow\psi_\downarrow\psi_\uparrow\right], \tag{7}$$

where $\beta=1/\left(k_BT\right)$, T is the temperature, and k_B is the Boltzmann constant. To allow for spin imbalance in the Fermi gas, chemical potentials μ_σ are introduced which can be different for "spin-up" and "spin-down" species. The coordinate dependent chemical potentials μ_σ are determined by (5) with $\mu_0\to\mu_{0,\sigma}$ for each component. The interaction energy with the coupling constant $g<0$ describes the model contact interactions between fermions as, for example, in Ref. [35]. It represents the Cooper pairing channel determined by the s-wave scattering between two fermions with antiparallel spins. The one-particle Hamiltonian H in the rotating frame of reference is determined by formula (1).

After performing the Hubbard-Stratonovich transformation which introduces the bosonic pair fields $\left(\bar{\Psi},\Psi\right)$, and integrating over the fermionic fields, the partition function becomes [2]

$$\mathcal{Z} \propto \int \mathcal{D}\left[\bar{\Psi},\Psi\right] e^{-S_{eff}}, \tag{8}$$

with the effective bosonic action S_{eff}:

$$S_{eff}=S_B-\mathrm{Tr}\left[\ln\left(-\mathbb{G}^{-1}\right)\right]. \tag{9}$$

We decompose the inverse Nambu matrix $\mathbb{G}^{-1}$ into a sum of the matrix $\mathbb{F}$ proportional to the pair field Ψ, as in Ref. [26],

$$\mathbb{F}\left(\mathbf{r},\tau\right)=\left(\begin{array}{cc} 0 & -\Psi\left(\mathbf{r},\tau\right) \\ -\bar{\Psi}\left(\mathbf{r},\tau\right) & 0 \end{array}\right),$$

and the free-field contribution,

$$\mathbb{G}_{0}^{-1}\left(\mathbf{r},\tau\right)=\left(\begin{array}{cc} -\frac{\partial}{\partial\tau}-H+\mu_{\uparrow} & 0 \\ 0 & -\frac{\partial}{\partial\tau}+H^{*}-\mu_{\downarrow} \end{array}\right). \tag{10}$$

In the momentum representation, the $\mathbb{G}_{0}$ is explicitly obtained from (10):

$$\mathbb{G}_{0}\left(\mathbf{k},n\right)=\left(\begin{array}{cc} \frac{1}{i\omega_{n}-\xi_{\mathbf{k}}+\zeta_{\mathbf{k}}} & 0 \\ 0 & \frac{1}{i\omega_{n}+\xi_{\mathbf{k}}+\zeta_{\mathbf{k}}} \end{array}\right) \tag{11}$$

with $\xi_{\mathbf{k}}=k^{2}/\left(2m\right)-\mu\left(\mathbf{r}\right)$ and

$$\zeta_{\mathbf{k}}=\zeta+\left(1/m\right)\mathbf{k}\cdot\mathbf{A}\left(\mathbf{r}\right), \tag{12}$$

where $\mu=\left(\mu_{\uparrow}+\mu_{\downarrow}\right)/2$ and $\zeta=\left(\mu_{\uparrow}-\mu_{\downarrow}\right)/2$. As discussed above, the coordinate-dependent vector potential is taken into account here in the local density approximation, assuming that $\mathbf{A}\left(\mathbf{r}\right)$ varies slowly, as does the trapping potential (which is included here through the coordinate dependent chemical potential). Hence, the effect of rotation on the effective field action functional derived in Ref. [26] is taken into account through the replacement of the chemical potential imbalance ζ to $\zeta_{\mathbf{k}}$. The above procedure is quite similar for Fermi gases in three and two dimensions. The coefficients in the effective field action in the rotating frame of reference (generalized here for a ν-dimensional Fermi gas with $\nu=2,3$) take the

form:

$$C = \int \frac{d^\nu \mathbf{k}}{(2\pi)^\nu} \frac{k^2}{\nu m} f_2\left(\beta, E_\mathbf{k}, \zeta_\mathbf{k}\right), \tag{13}$$

$$D = \int \frac{d^\nu \mathbf{k}}{(2\pi)^\nu} \frac{\xi_\mathbf{k}}{w} \left[f_1\left(\beta, \xi_\mathbf{k}, \zeta_\mathbf{k}\right) - f_1\left(\beta, E_\mathbf{k}, \zeta_\mathbf{k}\right)\right], \tag{14}$$

$$E = 2\int \frac{d^\nu \mathbf{k}}{(2\pi)^\nu} \frac{k^2}{\nu m} \xi_\mathbf{k}^2 \; f_4\left(\beta, E_\mathbf{k}, \zeta_\mathbf{k}\right), \tag{15}$$

$$\begin{aligned} Q = \frac{1}{2w}\int \frac{d^\nu \mathbf{k}}{(2\pi)^\nu} \left[f_1\left(\beta, E_\mathbf{k}, \zeta_\mathbf{k}\right)\right. \\ \left. - \left(E_\mathbf{k}^2 + \xi_\mathbf{k}^2\right) f_2\left(\beta, E_\mathbf{k}, \zeta_\mathbf{k}\right)\right], \end{aligned} \tag{16}$$

$$\begin{aligned} R = \int \frac{d^\nu \mathbf{k}}{(2\pi)^\nu} \left[\frac{f_1\left(\beta, E_\mathbf{k}, \zeta_\mathbf{k}\right) + \left(E_\mathbf{k}^2 - 3\xi_\mathbf{k}^2\right) f_2\left(\beta, E_\mathbf{k}, \zeta_\mathbf{k}\right)}{3w}\right. \\ \left. + \frac{4\left(\xi_\mathbf{k}^2 - 2E_\mathbf{k}^2\right)}{3} f_3\left(\beta, E_\mathbf{k}, \zeta_\mathbf{k}\right) + 2E_\mathbf{k}^2 w f_4\left(\beta, E_\mathbf{k}, \zeta_\mathbf{k}\right)\right], \end{aligned} \tag{17}$$

with $w = |\Psi|^2$. Correspondingly, the coordinate-dependent thermodynamic potential in the rotating frame of reference is determined by the expressions:

$$\begin{aligned} \Omega_s\left(w\right) = -\int \frac{d\mathbf{k}}{(2\pi)^3} \left(\frac{1}{\beta}\ln\left(2\cosh\beta E_\mathbf{k} + 2\cosh\beta\zeta_\mathbf{k}\right)\right. \\ \left. -\xi_\mathbf{k} - \frac{mw}{k^2}\right) - \frac{mw}{4\pi a_s} \quad \text{(in 3D)}, \end{aligned} \tag{18}$$

and

$$\begin{aligned} \Omega_s\left(w\right) = -\int \frac{d^2\mathbf{k}}{(2\pi)^2} \left(\frac{1}{\beta}\ln\left(2\cosh\beta E_\mathbf{k} + 2\cosh\beta\zeta_\mathbf{k}\right)\right. \\ \left. -\xi_\mathbf{k} - \frac{w}{2k^2 + E_b}\right) \quad \text{(in 2D)}, \end{aligned} \tag{19}$$

where E_b is the binding energy for a two-particle bound state in 2D.

For a balanced gas with $\zeta = 0$, rotation does not induce imbalance even though $\zeta_\mathbf{k} \neq 0$, since the contributions with $\zeta_\mathbf{k}$ and $\zeta_{-\mathbf{k}}$ cancel out in the integration over $\mathbf{k}$. However, this "local momentum imbalance" influences the background parameters, reducing the radius of the superfluid state in the trap and consequently leading to a critical (upper) rotation frequency above which superfluidity is fully suppressed. Moreover, this local momentum imbalance appears first in the Nambu tensor in full agreement with the Nambu-Gorkov theory. In order to see this, we can refer to the works [20, 21, 33], where the inverse Nambu matrix appears with the same one-particle Hamiltonian as in the present work.

The appearance of this "local momentum imbalance" is physically transparent. In a Cooper pair, the two fermions have opposite momenta. In the presence of rotation, their

single-particle energies become unequal, in the same way as two pairing electrons in the magnetic field experience a Zeeman splitting. Note that for Cooper-paired electrons in a magnetic field, the Lorentz force destabilizes the pair already at much lower magnetic field than that where the Zeeman splitting breaks up the pair – however, for the neutral atoms, this effect is absent. This physical picture assumes that the Cooper pair size is small with respect to a characteristic size of the superfluid system (for example, the radius of the trap) so that the background parameters within the extent of a Cooper pair are approximately uniform. This condition needs to be fulfilled in order for any description in terms of an effective field theory [24, 27, 29–31] to be applicable. It should be noted that whereas the aforesaid splitting of the fermion energy is a standard result for the Bogoliubov - de Gennes theory, it has not been taken into account in existing effective field theories, so that this seems to be new with respect to other EFT-like approaches.

In addition to the $\zeta \to \zeta_{\mathbf{k}}$ replacement, rotation leads to a new term in the effective field action, proportional to the first-order space gradient of the pair field. This term of the gradient expansion vanished in the absence of rotation due to inversion symmetry. However, in the presence of rotation it must survive. It is calculated as in Ref. [26], summing up the whole series in powers of the amplitude of the pair field in the coefficient of $\nabla\Psi$. The resulting effective field action takes the form:

$$\begin{aligned} S_{eff} = \int_0^\beta d\tau \int d\mathbf{r} \Bigg\{ \Bigg[& \Omega_s(w) + \frac{D}{2}\left(\bar{\Psi}\frac{\partial\Psi}{\partial\tau} - \frac{\partial\bar{\Psi}}{\partial\tau}\Psi\right) \\ & + Q\frac{\partial\bar{\Psi}}{\partial\tau}\frac{\partial\Psi}{\partial\tau} - \frac{R}{2w}\left(\frac{\partial w}{\partial\tau}\right)^2 + \frac{C}{2m}\left(\nabla_{\mathbf{r}}\bar{\Psi}\cdot\nabla_{\mathbf{r}}\Psi\right) - \frac{E}{2m}\left(\nabla_{\mathbf{r}}w\right)^2 \\ & + i\frac{G}{2m}\mathbf{A}\cdot\left(\bar{\Psi}\nabla_{\mathbf{r}}\Psi - \Psi\nabla_{\mathbf{r}}\bar{\Psi}\right)\Bigg]\Bigg\}. \end{aligned} \tag{20}$$

The new term ($\propto \mathbf{A}$) expresses the coupling of the vector potential to the current density. The coefficients D, C, E, Q, R in this effective field action are given by (13) to (17), and the new coefficient G (which appears due to the rotation) is:

$$\begin{aligned} G = & D \\ & + \int \frac{d^\nu\mathbf{k}}{(2\pi)^\nu}\frac{1}{w}\frac{(\mathbf{k}\cdot\mathbf{A})}{|\mathbf{A}|^2}\zeta_{\mathbf{k}}\left[f_1(\beta,\zeta_{\mathbf{k}},\xi_{\mathbf{k}}) - f_1(\beta,\zeta_{\mathbf{k}},E_{\mathbf{k}})\right]. \end{aligned} \tag{21}$$

The terms with the gradient of the pair field can be equivalently rewritten in terms of the

covariant derivatives,

$$\int d\mathbf{r}\left[\frac{C}{2m}\left(\nabla_{\mathbf{r}}\bar{\Psi}\cdot\nabla_{\mathbf{r}}\Psi\right)+i\frac{G}{2m}\mathbf{A}\cdot\left(\bar{\Psi}\nabla_{\mathbf{r}}\Psi-\Psi\nabla_{\mathbf{r}}\bar{\Psi}\right)\right]$$
$$=\int d\mathbf{r}\left[\frac{C}{2m}\left|\left(\nabla_{\mathbf{r}}-i\mathring{e}\mathbf{A}\right)\Psi\right|^{2}-\frac{C}{2m}\mathring{e}^{2}A^{2}\left|\Psi\right|^{2}\right], \tag{22}$$

with the factor $\mathring{e}=G/C$. As established in Ref. [26] the coefficient D enters the equations of motion for the pair fields only through the combination $\tilde{D}\equiv\partial\left(wD\right)/\partial w$. Thus the coefficient D is determined up to an arbitrary term proportional to w^{-1}. The same is true for the coefficient G: it enters the equations of motion through the parameter $\tilde{G}\equiv\partial\left(wG\right)/\partial w$. Consequently, physical sense can be attributed to the factor

$$\tilde{e}=\frac{\tilde{G}}{C}.$$

If $\mathbf{A}$ were an electromagnetic vector potential, $\tilde{e}$ could be interpreted as the ratio between the charge of the pair and the charge of a single fermion. In the Ginzburg - Landau formalism for superconductors, the pair has twice the charge of a single electron. Here, $\mathbf{A}$ is a rotational vector potential, so we will refer to $\tilde{e}$ as the "rotational charge". This quantity also represents the ratio of the rotational moment of inertia of the pair to that of a single fermion. In the BEC limit, the pairs are tightly bound, and we can treat them as point particles with mass $2m$ and rotational moment of inertia $2mr^{2}$. Hence, in this limit we expect $\tilde{e}=2$. However, moving away from the BEC limit, the pair becomes delocalized (naively speaking, for the pair field $\Psi\left(\mathbf{r}\right)$, both fermions are no longer located at the same position $\mathbf{r}$), and the pair mass also rescales proportional to C^{-1}. Hence, we expect $\tilde{e}$ to deviate from its BEC value of 2.

In Fig. 1, $\tilde{e}$ is plotted as a function of the inverse scattering length $1/\left(k_{F}a_{s}\right)$ and the temperature, when T passes from zero to T_{c} for a three-dimensional Fermi gas confined to a cylindrically symmetric parabolic confinement potential, with the number of particles per unit length set to $N=1000$. We use the set of units with $\hbar=1$, $m=1/2$, and the Fermi energy for a free-particle Fermi gas $E_{F}\equiv\hbar^{2}k_{F}^{2}/\left(2m\right)=1$, where $k_{F}\equiv\left(3\pi^{2}n\right)^{1/3}$ is the Fermi wave vector and n is the fermion density. As seen from Fig. 1, $\tilde{e}$ only slightly depends on the temperature, and tends to 2 in the BEC limit as expected. Moving away from the BEC limit, it gradually diminishes. The obtained behavior of the "rotational charge" differing from the *ad hoc* value $\tilde{e}=2$ is one of the key results of the present approach, which was never derived in preceding works using effective field theories.

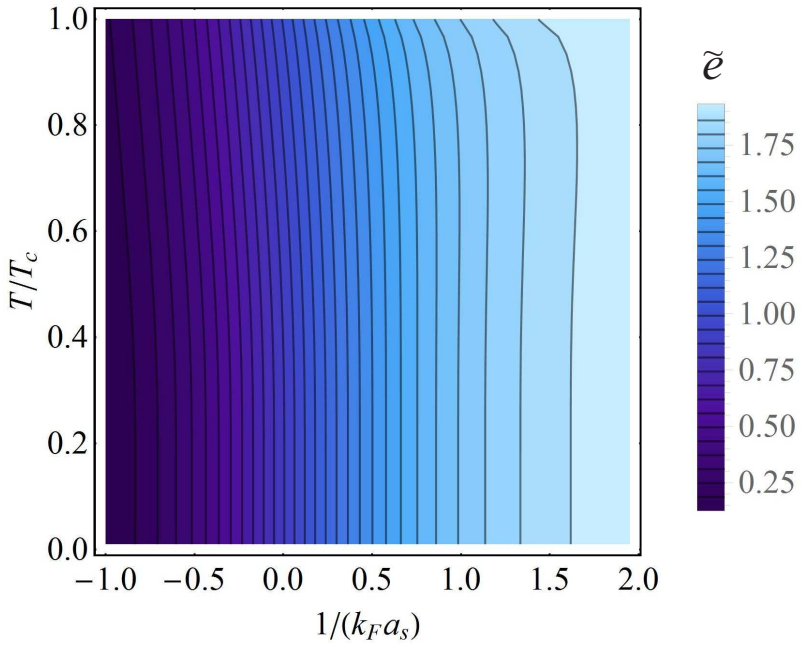

FIG. 1: (color online). "Rotational charge" $\tilde{e}$ as a function of the inverse scattering length $1/\left(k_F a_s\right)$ and the relative temperature T/T_c for a three-dimensional Fermi gas in a cylindricaly symmetric parabolic confinement potential, with the number of particles per unit length $N = 1000$.

In the derivation presented above, we start from the action for the fermionic field ψ in the lab frame, then transform it to the rotating frame of reference, and finally perform the Hubbard-Stratonovich transformation to introduce the pair field Ψ. As an alternative approach, one could consider inverting the order of these operations: first obtaining the action for the pair field Ψ in gradient expansion, and then applying the transformation to the rotating frame of reference. In that case, a term $(-\omega L_z)$ appears in the bosonic pair Hamiltonian similarly as in the Gross-Pitaevskii theory [2], where $\hat{L}_z$ is the z component of the orbital angular momentum of a bosonic pair described by the field Ψ. This alternative order of operations leads to the same final result as obtained above (20)-(22), but with the rotational charge of the pair given by $\tilde{e} = \tilde{D}/C$.

This can be understood by writing the energies entering expression (11) for $\mathbb{G}_0$ as follows:

$$\xi_{\mathbf{k}} \pm \zeta_{\mathbf{k}} = \frac{\left(\mathbf{k} \pm \mathbf{A}\right)^2}{2m} - \mu_\omega \pm \zeta. \tag{23}$$

Here the chemical potential μ_ω is determined by (5) and completely accounts for the renormalization of the confinement potential due to rotation. The other contribution – a shift

of the fermion momentum $\mathbf{k}$ due to the vector potential – must be small within the range of applicability of the effective field theory. The physical grounds for this conclusion are in accordance with the key assumption common to any effective field theory: the pair field is slowly varying in space and time with respect to the fermionic variables. Therefore also the rotational vector potential $\mathbf{A}$ must vary slowly with respect to the fermionic variables. Hence we can assume that in (23), $\mathbf{A}$ is small with respect to $\mathbf{k}$. If one neglects $\mathbf{A}$ in (23), the parameters (13)-(19) of the effective field action keep the same form with the replacements of $\zeta_{\mathbf{k}}$ by ζ and of $\xi_{\mathbf{k}} = k^2/(2m) - \mu$ by $\xi_{\mathbf{k}} = k^2/(2m) - \mu_\omega$. Correspondingly, in this approximation $G = D$, and the rotational charge of a pair indeed becomes $\tilde{e} = \tilde{D}/C$. Thus, the approach when first making the gradient expansion and then introducing rotation corresponds to neglecting $\mathbf{A}$ in (23). Within the range of applicability of the EFT as determined in Refs. [26, 28], the difference between the results obtained using these two approaches is very small. The subsequent numeric calculation in the present work is performed using the second of two aforesaid approximations.

Finally, note that the effective field action for a two-band system is straightforwardly determined in the same way as in Ref. [26]. We obtain action functionals for the separate fields, and a coupling given by an interband Josephson term:

$$S_{eff}^{(2b)} = \sum_{j=1,2} S_{eff}^{(j)} - \int_0^\beta d\tau \int d\mathbf{r}\, \frac{\sqrt{m_1 m_2}}{4\pi} \gamma \left(\bar{\Psi}_1 \Psi_2 + \bar{\Psi}_2 \Psi_1 \right), \tag{24}$$

Here $S_{eff}^{(j)}$ is the single-band effective field action for the j-th band determined by (20) with $j = 1, 2$, and γ is the strength of the interband coupling, fixed by the scattering lengths.

III. VORTEX FORMATION

In order to study the formation of vortices and vortex pairs in rotated superfluid Fermi gases, we use the amplitude-phase representation for the pair field similarly as in Refs. [27, 28],

$$\Psi(\mathbf{r}) = |\Psi_\infty|\, a(\mathbf{r})\, e^{i\theta(\mathbf{r})}. \tag{25}$$

In this expression, $|\Psi_\infty|$ is the uniform background amplitude determined by solving gap and number equations for the uniform system. The amplitude modulation (the "hole" in the modulus of the order parameter at the vortex core) is modeled by the real function $a(\mathbf{r})$.

The phase pattern is taken into account by $\theta(\mathbf{r})$ – for a vortex aligned with the z-axis, this is the angle around the z-axis. With this representation for Ψ, the free energy corresponding to the effective action becomes

$$F = \int d\mathbf{r} \left\{ \sum_{j=1,2} \left[\Omega_s(w) + \frac{1}{2}\rho^{(qp)} \left(\nabla_{\mathbf{r}} a\right)^2 \right] + \frac{1}{2}\rho^{(sf)} a^2 \left(\nabla_{\mathbf{r}}\theta - \mathring{e}\mathbf{A}\right)^2 - \frac{1}{2}\rho^{(sf)} \left(a\mathring{e}\mathbf{A}\right)^2 \right\}, \tag{26}$$

with

$$\rho^{(sf)} = \frac{C}{m} \left|\Psi_\infty\right|^2, \tag{27}$$

$$\rho^{(qp)} = \frac{C - 4E}{m} \left|\Psi_\infty\right|^2. \tag{28}$$

The parameters $\rho^{(sf)}$ and $\rho^{(qp)}$ represent, respectively, the superfluid density and the quantum pressure coefficient, as established in Refs. [26, 27]. In order to find the conditions of stability for the vortex solutions, we consider the difference between two free energies:

$$\delta F \equiv F_{vortex} - F_0 \tag{29}$$

where F_{vortex} and F_0 are given by (26), respectively, with and without vortices. The bounds for the phase diagrams with several vortex configurations are determined from the comparison of the free energies corresponding to these configurations.

From here on, we focus on vortex stability conditions for a one-band Fermi gas in three dimensions, trapped in a cylindrically symmetric parabolic potential characterized by the confinement frequency ω_0, and rotating around the symmetry axis at a frequency ω. We do not consider at the present stage the case when the population imbalance ζ is other than zero. The area of existence of vortices lies, in general, inside the area of existence for a superfluid state in a rotating Fermi gas. The latter one extends from the zero rotation frequency $\omega = 0$ to a critical rotation frequency for the superfluid state $\omega_{\max} < \omega_0$. For $\omega > \omega_{\max}$, the system turns into the normal state [33, 36, 37].

For a non-rotating Fermi gas and at sufficiently low rotation frequencies, vortices are not stable as long as the free energy (26) without vortices is lower than the free energy with vortices. When increasing ω, vortices can become stable starting from a certain critical rotation frequency $\omega = \omega_{c,1}$. There may exist also an upper critical rotation frequency

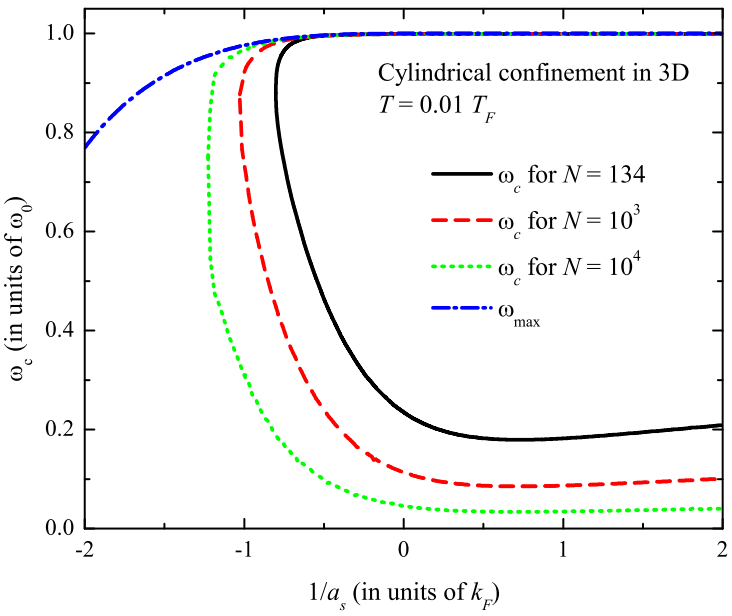

FIG. 2: (color online). Area of existence for vortices for a Fermi gas trapped in a cylindrically symmetric parabolic potential at $T = 0.01T_F$, with different numbers of particles per unit length.

$\omega_{c,2} < \omega_{\max}$ such that the vortex state turns back to the superfluid state for $\omega_{c,2} < \omega < \omega_{\max}$, since the radius of the superfluid state falls down with an increasing rotation frequency [21].

The area of existence for vortices for a system with different numbers of particles N per unit length at $T = 0.01T_F$ (where $T_F = E_F/k_B$) is shown in Fig. 2. The value $N = 134$ corresponds to $\mathcal{N} = 1000$ in Ref. [21], where the unit length is chosen as $(\hbar/(m\omega_0))^{1/2}$. We do not perform a quantitative comparison of the phase diagrams calculated within the current approach with the phase diagrams obtained by the BdG method [21] since the study in Ref. [21] has been performed for the far BCS regime and at $T = 0$, where the quantitative results of the current effective field theory, as discussed in Refs. [26, 27], are hardly applicable. Nevertheless, the qualitative behavior of the phase boundary for the formation of stable vortices is in agreement with the predictions of the BdG theory even in the BCS side. Particularly, we can see a bend-over of the critical rotation frequency and hence the existence of both a lower and an upper critical rotation frequency at weak coupling. At higher coupling strengths, the upper critical rotation frequency for the vortex formation tends to the critical rotation frequency for the superfluid state.

The region of vortex stability extends deeper into the BCS side and to smaller values of $\omega_{c,1}$ when increasing the number of particles. For sufficiently large $N \gtrsim 10^4$, stable

vortices as predicted by the current formalism can be observed in the entire experimentally available BCS-BEC crossover region ($-1.2 < 1/(k_F a_s) < 3.8$), in line with the experimental observations [8]. We have checked numerically that the lower critical rotation frequency $\omega_{c,1}$ for a single vortex in a Fermi gas with a large number of particles behaves in accordance with the estimation [11, 38]:

$$\omega_{c,1}|_{N\gg 1} \propto \omega_B \equiv \frac{1}{R_c^2} \ln\left(\frac{R_c}{\xi}\right), \tag{30}$$

where R_c is the radius of the superfluid state in a trap, and ξ is the healing length which characterizes the vortex size. The result of this numerical check is shown in Fig. 3. It shows the lower critical rotational frequency for a Fermi gas as a function of the number of particles per unit length and the ratio of the critical frequency compared to the analytic expression (30). We see that the ratio $\omega_{c,1}/\omega_B$ only slightly varies when N passes from $N = 10$ to $N = 100$, so that the asymptotic trend (30) is clearly visible already when N is not very large.

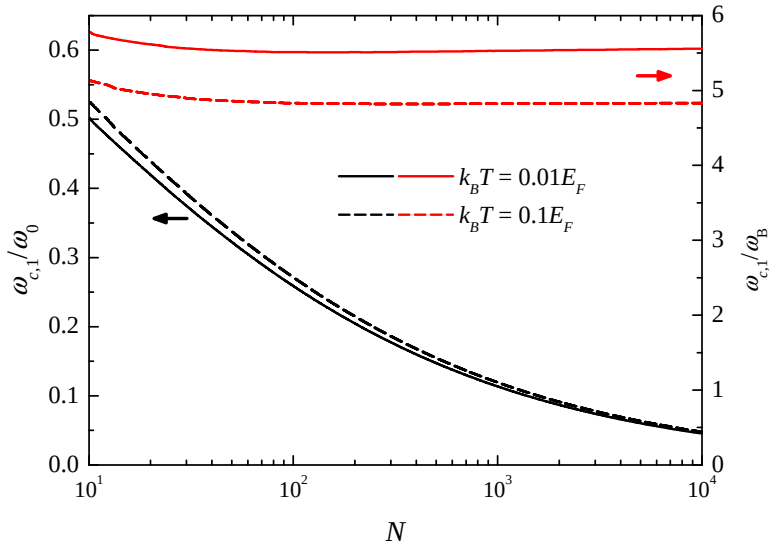

FIG. 3: (color online). *Left-hand axis*: the lower critical rotation frequency $\omega_{c,1}$ (in units of the trapping potential parameter ω_0) for a trapped Fermi gas as a function of the number of particles per unit length for $1/(k_F a_s) = 0$, at two temperatures $k_B T = 0.01 E_F$ and $k_B T = 0.1 E_F$. *Right-hand axis*: the ratio ω_c/ω_B where ω_B is given by formula (30).

A similar asymptotic dependence for a Fermi gas trapped to a 3D spherically symmetric confinement potential was predicted in Ref. [11] for a Fermi gas at zero temperature. In the

present treatment, we find that the trend (30) is kept also at finite temperatures.

We can compare the obtained critical rotation frequency with the LPDA results of Ref. [23], using the parameters of the experimental setup of Ref. [39] where the unitary Fermi gas $[1/(k_F a_s) = 0]$ is trapped to an elongated trap with the confinement frequencies $\omega_\perp \approx 2\pi \times 680\,\mathrm{Hz}$ and $\omega_z \approx 2\pi \times 24\,\mathrm{Hz}$. When approximating this setup by a cylindrical confinement potential, we arrive at the number of particles per unit length $N \sim 10^4$. As seen from Fig. 3, for this number of particles, $\omega_{c,1} \approx 0.045$, which is in good agreement with the lower critical rotation frequency obtained in Ref. [23].

When the rotation frequency is increased beyond $\omega_{c,1}$, a second vortex may enter the superfluid. In the phase diagram of Fig. 4, we distinguish the superfluid states with no vortex, one vortex and two or more vortices, in a trapped Fermi gas with $N = 1000$ at the temperature $T = 0.1T_F$. This temperature is higher than that for Fig. 2, and as a consequence the BCS-side phase boundary for vortex formation is found to shift to stronger coupling strengths. The boundary between the regimes with one and two vortices behaves similarly to the critical rotation frequency for a single vortex. It also exhibits a bend-over. The lower critical rotation frequency for a vortex pair is higher than the lower critical rotation frequency for a single vortex. On the contrary, the upper critical rotation frequency for a vortex pair is lower than the higher critical rotation frequency for a single vortex. Also the weak-coupling bound of $1/a_s$ for a single vortex lies more towards the BCS side with respect to that for a vortex pair Thus the area where two or more stable vortices can exist lies entirely inside the area of stability for a single vortex.

Fig. 5 shows the behavior of the radius of the superfluid state R_c and the half-distance between vortex centers R_v for a vortex pair (inset) as a function of the relative rotation frequency ω/ω_0 for a rotating Fermi gas with $1/a_s = 0$ and $N = 10^3$ confined to a cylindrically symmetric parabolic potential. The dependence of the radius of the superfluid state versus ω is non-monotonic. When rotation gradually becomes faster but ω is not yet very close to its critical value $\omega_{\max} < \omega_0$ (where the superfluid state disappears), R_c slowly increases, because the confinement weakens due to the centrifugal force. When ω is sufficiently close to $\omega_{\max}$, the superfluid core shrinks, turning to zero at $\omega = \omega_{\max}$. The critical value $\omega_{\max}$ decreases with increasing temperature, in accordance with the predictions of other works [21, 37].

Fig. 5 allows us to see also the temperature dependence of the size of the superfluid state

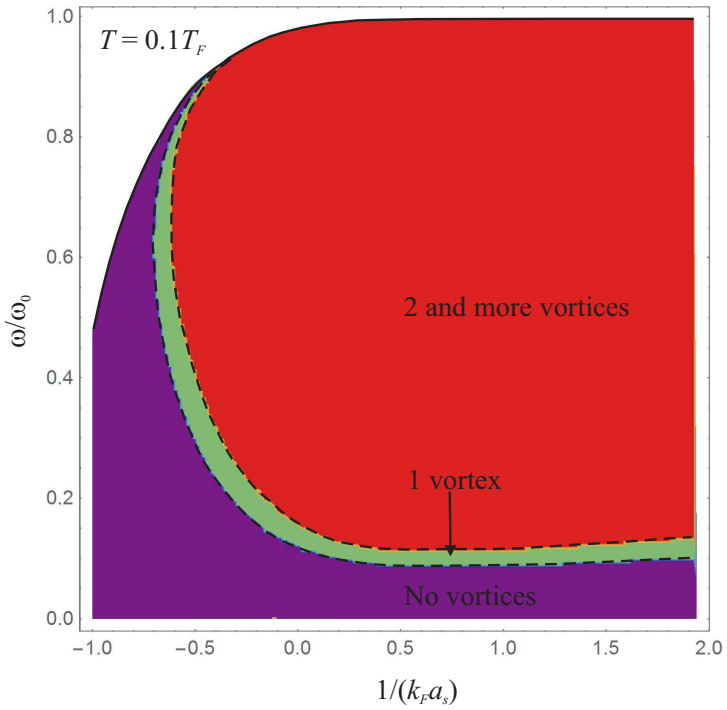

FIG. 4: (color online). Phase diagram for a trapped rotating Fermi gas in a cylindrically symmetric parabolic confinement potential, showing the critical rotation frequencies as a function of the inverse scattering length for $T = 0.1T_F$ and the number of particles per unit length $N = 10^3$. The critical rotation frequencies are plotted for a single vortex and for a vortex pair. Also the upper bound for the rotation frequency is shown, which restricts the area of existence for the superfluid state.

and of the half-distance for the vortex pair. When ω is not close enough to $\omega_{\max}$, the radius R_c decreases rather slowly with rising temperature. In the vicinity of $\omega_{\max}$, this decrease becomes much faster. The half-distance between vortices for a pair weakly depends on the temperature, except near $\omega_{\max}$, where R_v falls together with R_c.

In Fig. 6, we plot the vortex phase diagrams as a function of the variables $(\omega/\omega_0, T/T_F)$ for two fixed interaction strengths $1/(k_F a_s) = -0.5$ and $1/(k_F a_s) = 0$, and for two numbers of particles per unit length $N = 10^3$ and $N = 10^4$ (explicitly shown in the figure). Also in this phase diagram the transition lines between the regimes with no vortex, one vortex, and two or more vortices bend over leading to reentrant behavior of the critical rotation frequencies as a function of temperature. This reentrant dependence has a clear physical sense. On one hand, at higher temperatures, the radius of the superfluid phase (which is surrounded by the normal phase) decreases. On the other hand, the healing length, which

determines the vortex size, increases when the temperature rises towards T_c. When the healing length is sufficiently large, the existence of stable vortices becomes energetically non-favorable with respect to the superfluid state.

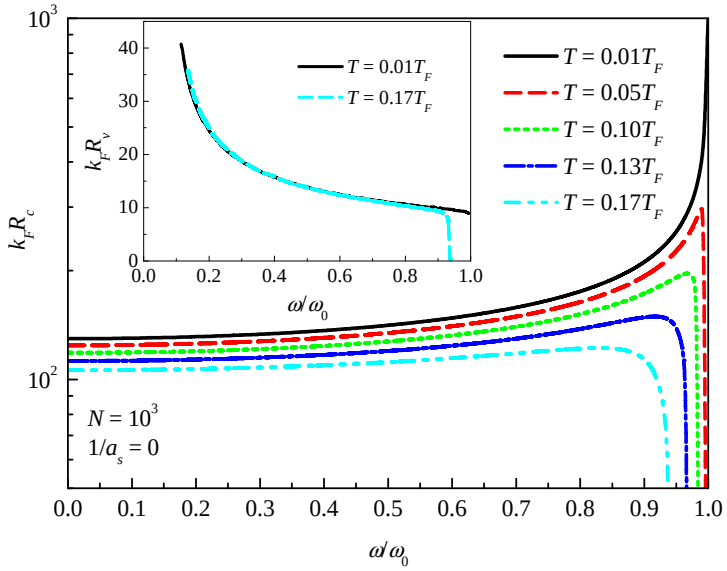

FIG. 5: (color online). Radius of the superfluid state as a function of the rotation frequency for a rotating Fermi gas with $1/a_s = 0$ and $N = 10^3$ confined to a cylindrically symmetric parabolic potential, at different temperatures. Inset shows the half-distance between vortex centers for a vortex pair at two temperatures.

The obtained phase diagrams exhibit a clear similarity to those obtained in Ref. [21] (where they are calculated in the far BCS regime and at lower temperatures than those considered in the present work) and in Ref. [23]. In particular, the phase diagram shown in Fig. 6 (d) corresponds to the same experimental setup as in Ref. [39] theoretically considered in Ref. [23]. We note a good agreement of the critical rotation frequencies in Fig. 6 (d) with those in the phase diagram calculated within LPDA and shown in Fig. S 2 of the Supplement to Ref. [23]. There are however some important differences. In the BdG method, there is an uncertainty between two definitions of the lower critical rotation frequency. A lower value of $\omega_{c,1}$ corresponds to the critical angular frequency at which an isolated vortex placed initially close to the trap center is attracted toward the trap center, while the upper value of $\omega_{c,1}$ corresponds to the critical rotation frequency at which an isolated vortex placed initially at the edge is attracted toward the trap center. This uncertainty is apparently related to the

fact that the LPDA equation can hardly be considered as a result of the least action principle for a GL-like action functional or the variational principle for a GL-like free energy [40]. On the contrary, the effective action functional (20) is well-determined, and the condition for the vortex formation directly follows from the comparison of the free energies with and without vortices. Therefore the aforesaid uncertainty does not appear in the present work. According to the results shown in Fig. 3, the critical rotation frequency $\omega_{c,1}$ given by the present EFT is very close to the lowest of two values of $\omega_{c,1}$ provided by the coarse grained BdG theory [23]. This may resolve the uncertainty between two values of $\omega_{c,1}$ indicated in Ref. [23]: only the lowest one of them seems to be true. This can be supported also by the physical reasoning, since, when gradually increasing the rotation frequency, a single stable vortex can appear when ω passes $\omega_{c,1}$. After this, the second (higher) value of $\omega_{c,1}$ has no significance: the stable vortex state already exists.

A comparison with the observations of vortices in the experiment of Ref. [8] indicates that the ranges of applicability of the BdG formalism combined with the Thomas-Fermi approximation [20, 21] and the KTD effective field theory are complementary to each other. The KTD field theory becomes more accurate towards the BEC regime [26], while, as concluded in Ref. [21], the BdG method is quantitatively more reliable towards the BCS regime. It was found in Refs. [20, 21] that within the BdG theory, vortices in rotating Fermi gases are formed only for relatively large negative scattering lengths. On the contrary, the current formalism predicts the formation of stable vortices in rotating Fermi gases in the whole BCS-BEC crossover, in agreement with the experimental observations [8].

The inverse scattering length was varied in the experiment of Ref. [8] in a wide range from $1/\left(k_F a_s\right) = -1.2$ to $1/\left(k_F a_s\right) = 3.8$, and vortices were observed in the whole range of $1/\left(k_F a_s\right)$ between those values. In the experiment [8], ^{6}Li atoms were trapped in an approximately parabolic trap with the confinement frequencies $\omega_\perp \approx 2\pi \times 57\,\mathrm{Hz}$ and $\omega_z \approx 2\pi \times 23\,\mathrm{Hz}$. This gives us an estimation of the trap length along the z axis $l_z \equiv \left(\hbar/\left(m\omega_z\right)\right)^{1/2} \approx 8.5\,\mu\mathrm{m}$. The total number of atoms was $N \propto 10^6$. Thus we can estimate the number of particles per unit length in order to qualitatively match the experiment as $N \propto N/l_z \propto 10^4$. The highest number of vortices at a given stirring frequency was obtained at $1/\left(k_F a_s\right) \approx 0.35$ which is rather close to the position of the minimum of the critical rotation frequency for $N = 10^4$ in Fig. 2. It is hard to extract the critical rotation frequency for a single vortex from the experimental data of Ref. [8]. However, it is suggestive that the minimum of the critical

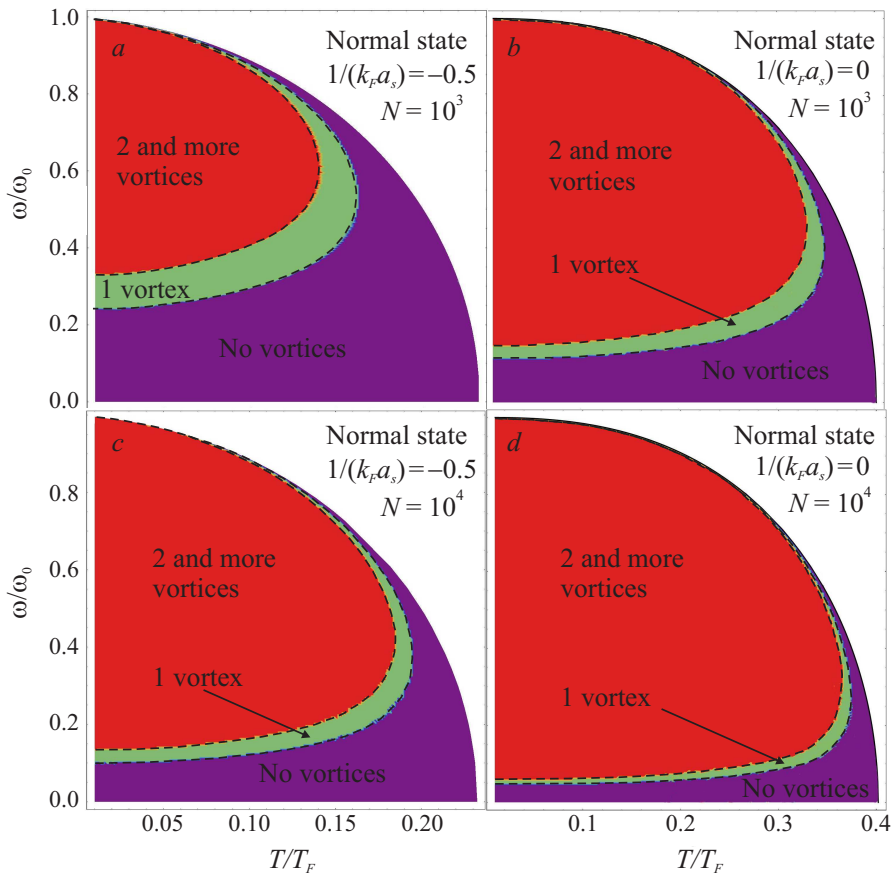

FIG. 6: (color online). Phase diagrams for a trapped rotating Fermi gas in a cylindrically symmetric parabolic confinement potential, showing the critical rotation frequencies as a function of the temperature for two numbers of particles per unit length and two inverse scattering lengths (indicated in the figure). The notations are the same as in Fig. 4.

rotation frequency and the maximum of vortices at a given (higher) rotation frequency lie close each other. Thus the above results of the present work are in line with the experiment [8] in what concerns the most favorable scattering length for the vortex formation in a rotating Fermi gas. Also, the estimate of the optimal rotation frequency within the modified finite temperature EFT is in a good agreement with the result of the coarse grained BdG theory [23]. This agreement is remarkable despite the fact that the rotation is incorporated in the LPDA equation of Ref. [23] similarly to the magnetic field, with the "rotational charge" equal to 2. The optimal value of the inverse scattering length for the generation of vortices is related to a sufficiently strong coupling regime, where, as seen from Fig. 1, $\tilde{e}$ is relatively close to 2. This explains the agreement between the present theory and LPDA in

the interpretation of the experimental results [8]. For weaker couplings, however, we expect more significant difference between results of these two theories.

IV. CONCLUSIONS

In the present work, we extend the effective field theory developed in Refs. [25, 26] for fermionic superfluids to the case of rotating Fermi gases. The rotation leads to a shift in the local chemical potential μ_ω, and to the appearance of a rotational vector potential $\mathbf{A}$ in the covariant derivative $-i\nabla_{\mathbf{r}} \to -i\nabla_{\mathbf{r}} - \mathring{e}\mathbf{A}$, that leads to the "rotational charge" $\tilde{e}$ in the equations of motion for the pair field. The rotational charge is related to ratio of the moment of inertia of the pair to that of the fermions, and goes to 2 in the BEC limit. However, moving away from the BEC limit, this value diminishes. We also find that when the gradient expansion is performed before the switch to the rotational frame of reference, a different value for $\tilde{e}$ is obtained, that difference is negligibly small within the range of applicability of the theory. The obtained distinction of the rotational charge from the ad hoc phenomenological value $\tilde{e} = 2$ has a clear physical explanation. The fermion pair in a rotating Fermi condensate moves similarly to a point particle only in the deep BEC regime. However, beyond the BEC limit, the fermion pair cannot be considered as a point particle, especially in the BCS regime, where the Cooper-pair size is large. As a result, the rotational charge diminishes when the inverse scattering length moves from BEC to the BCS side. This result demonstrates that the analogy between the external magnetic field and the rotation is not complete within an effective field approach.

Using the obtained formalism, we investigate phase diagrams where we identify regions for the superfluid state with no vortices, one vortex and two or more vortices. For the vortex phase diagrams in the variables $(\omega, 1/a_s)$, the transition curves between these regions bend over in the BCS regime, in agreement with the results found using BdG calculations in this regime [21]. As the number of particles is increased, the region of the phase diagram where vortices are stable extends deeper into the BCS regime. Increasing the temperature, on the other hand, shrinks the region of stable vortices. The obtained dependence of the rotational charge on the inverse scattering length is essential for these phase diagrams, especially for sufficiently weak couplings.

The vortex phase diagrams in the variables (ω, T) exhibit clear similarity with the results

of the BdG method (both the complete BdG [20, 21] and the coarse graining approximation for BdG [23]) where a good quantitative agreement has been found between the critical rotation frequencies obtained within the present theory and coarse-grained BdG. We have also arrived at the optimal inverse scattering length for the vortex formation corresponding to the lowest critical rotation frequency. This value of the inverse scattering length is in a good agreement with the coupling strength at which the maximal number of vortices is generated in the experiment [8].

It is worth noting that an advantage of the present method with respect to the BdG theory is much shorter computational time and lower memory consumption. This advantage persists even with respect to the coarse-grained BdG, because the minimization of the free energy is substantially simpler and faster than a numerical solution of the differential equations. Moreover, effective field approaches allow for analytic solutions in many interesting cases, as shown in our work on dark solitons [27]. Therefore it is planned to extend the treatment of non-linear excitations in condensed Fermi gases within the EFT, involving other factors of interest, such as spin imbalance, two-band Fermi gases, and spin-orbit coupling. The spin imbalance has been already incorporated analytically in the coefficients of the effective action (20), and the analysis of effects provided by the imbalance combined with the rotation is in progress. The spin-orbit coupling will be taken to account at the microscopic level similarly to Refs. [41]. Finally, as shown in Sec. II, the extension of the present approach to two-band Fermi gases is straightforward.

Acknowledgments

This research was supported by the Flemish Research Foundation (FWO-Vl), project nrs. G.0115.12N, G.0119.12N, G.0122.12N, G.0429.15N, by the Scientific Research Network of the Research Foundation-Flanders, WO.033.09N, and by the Research Fund of the University of Antwerp.

---

[1] I. Bloch, J. Dalibard, and W. Zwerger, Rev. Mod. Phys. **80**, 885 (2008).

[2] H. T. C. Stoof, K. B. Gubbels, and D. B.M. Dickerscheid, *Ultracold Quantum Fields* (Springer, 2009).

[3] M. Iskin and E. Tiesinga, Phys. Rev. A **79**, 053621 (2009).

[4] M. R. Matthews, B. P. Anderson,P. C. Haljan, D. S. Hall, C. E.Wieman, and E. A. Cornell, Phys. Rev. Lett. **83**, 2498 (1999).

[5] K. W. Madison, F. Chevy, W. Wohlleben, and J. Dalibard, Phys. Rev. Lett. **84**, 806 (2000).

[6] C. Raman, J.R. Abo-Shaeer, J.M. Vogels, K. Xu, and W. Ketterle, Phys. Rev. Lett. **87**, 210402 (2001).

[7] J. R. Abo-Shaeer, C. Raman, J. M. Vogels, and W. Ketterle, Science **292**, 476 (2001).

[8] M. W. Zwierlein, J. R. Abo-Shaeer, A. Schirotzek, C. H. Schunck, and W. Ketterle, Nature (London) **435**, 1047 (2005)

[9] M. Tsubota, K. Kasamatsu, and M. Ueda, Phys. Rev. A **65**, 023603 (2002).

[10] A. L. Fetter, Rev. Mod. Phys. **81**, 647 (2009).

[11] G. M. Bruun and L. Viverit, Phys. Rev. A **64**, 063606 (2001).

[12] M. Machida and T. Koyama, Phys. Rev. Lett. **94**, 140401 (2005).

[13] R. Sensarma, M. Randeria, and T.-L. Ho, Phys. Rev. Lett. **96**, 090403 (2006).

[14] C-C. Chien, Y. He, Q. Chen, and K. Levin, Phys. Rev. A **73**, 041603 (2006).

[15] S. Simonucci, P. Pieri, and G. C. Strinati, Phys. Rev. B **87**, 214507 (2013).

[16] A. Bulgac, Annu. Rev. of Nucl. Part. Sci. **63**, 97 (2013).

[17] F. Dalfovo and S. Stringari, Phys. Rev. A **53**, 2477 (1996).

[18] M. Cozzini and S. Stringari, Phys. Rev. Lett. **91**, 070401 (2003).

[19] M. Urban, Phys. Rev. A **71**, 033611 (2005).

[20] H. J. Warringa and A. Sedrakian, Phys. Rev. A **84**, 023609 (2011).

[21] H. J. Warringa, Phys. Rev. A **86**, 043615 (2012).

[22] R. Wei and E. J. Mueller, Phys. Rev. Lett. **108**, 245301 (2012).

[23] S. Simonucci1, P. Pieri, and G. Calvanese Strinati, Nature Physics **11**, 941 (2015).

[24] S. Simonucci and G. C. Strinati, Phys. Rev. B **89**, 054511 (2014).

[25] S. N. Klimin, J. Tempere, and J. T. Devreese, Physica C **503**, 136 (2014).

[26] S. N. Klimin, J. Tempere and J. T. Devreese, Eur. Phys. Journal B **88**, 122 (2015).

[27] S. N. Klimin, J. Tempere, and J. T. Devreese, Phys. Rev. A **90**, 053613 (2014).

[28] G. Lombardi, W. Van Alphen, S. N. Klimin, and J. Tempere (*to be published, arXiv:1506.02527*).

[29] M. Marini, F. Pistolesi, and G. C. Strinati, Eur. Phys. J. B **1**, 151 (1998).

[30] Y. Nishida and D. T. Son, Phys. Rev. A **74**, 013615 (2006).

[31] A. M. J. Schakel, Ann. Phys. **326**, 193 (2011).

[32] M. Gao, H. Wu, and L. Yin, Phys. Rev. A **74**, 023604 (2006).

[33] M. Urban and P. Schuck, Phys. Rev. A **78**, 011601 (R) (2008).

[34] L. P. Gor'kov, Sov. Phys. JETP **36**, 1364 (1959).

[35] C. A. R. Sá de Melo, M. Randeria, and J.R. Engelbrecht, Phys. Rev. Lett. **71**, 3202 (1993).

[36] I. Bausmerth, A. Recati, and S. Stringari, Phys. Rev. Lett. **100**, 070401 (2008).

[37] M. Y. Veillette, D. E. Sheehy, L. Radzihovsky, and V. Gurarie, Phys. Rev. Lett. **97**, 250401 (2006).

[38] N. Nygaard, G. M. Bruun, B. I. Schneider, C. W. Clark, and D. L. Feder, Phys. Rev. A **69**, 053622 (2004)..

[39] S Riedl, E. R. Sánchez Guajardo, C. Kohstall, J. Hecker Denschlag, and R Grimm, New J. Phys. **13**, 035003 (2011).

[40] As long as the coefficient at $|\nabla\Psi|^2$ in a GL-like free energy is coordinate-dependent, it necessarily leads to an equation which contains the first-order gradients of $\Psi(\mathbf{r})$ besides the second-order gradients.

[41] J. P. A. Devreese, J. Tempere, and C. A. R. Sá de Melo, Phys. Rev. Lett. **113**, 165304 (2014); Phys. Rev. A **92**, 043618 (2015).